Temperature-dependent Néel wall dynamics in GaMnAs/GaAs

2010 New J. Phys. 12 093022

(http://iopscience.iop.org/1367-2630/12/9/093022)

New Journal of Physics
The open-access journal for physics

Temperature-dependent Néel wall dynamics in GaMnAs/GaAs

J Honolka[1,3], L Herrera Diez[1], R K Kremer[1], K Kern[1], E Placidi[2] and F Arciprete[2]

[1] Max-Planck-Institut für Festkörperforschung, Heisenbergstrasse 1, 70569 Stuttgart, Germany
[2] Dipartimento di Fisica, Università di Roma 'Tor Vergata' and CNR-INFM, Via della Ricerca Scientifica 1, I-00133 Roma, Italy
E-mail: j.honolka@fkf.mpg.de

New Journal of Physics **12** (2010) 093022 (17pp)
Received 1 July 2010
Published 15 September 2010
Online at http://www.njp.org/
doi:10.1088/1367-2630/12/9/093022

Abstract. Extensive Kerr microscopy studies reveal strongly temperature-dependent domain wall (DW) dynamics in Hall bars made from compressively strained GaMnAs. Depending on the temperature, magnetic charging of the DWs is observed, and the nucleation rates depend on the Hall geometry with respect to the crystal axes. Above a critical temperature where a biaxial-to-uniaxial anisotropy transition occurs, a drastic increase in nucleation events is observed. Below this temperature, the nucleation of domains tends to be rather insensitive to temperature. This spatially resolved study of the DW dynamics in patterned GaMnAs at variable temperature has important implications for potential applications in single DW magneto-logic devices made from ferromagnetic semiconductors.

[3] Author to whom any correspondence should be addressed.

Contents

The ferromagnetic semiconductor GaMnAs [1] has been extensively studied in the past few years not only from the viewpoint of basic science but also focusing on the properties that can lead to novel applications in spin-based electronics and magneto-logic devices [2, 3]. For the latter, a good understanding of domain wall (DW) dynamics is needed in order to control processes such as DW nucleation and propagation. In ferromagnetic GaMnAs with in-plane magnetization, magnetic reversal processes have been studied mostly by means of magneto-transport [4, 5], but with very limited gain of local information about DW nucleation and motion. Magnetic domains in GaMnAs/GaAs were first observed magneto-optically with the aid of a garnet film as an optical magnetic field sensor where large domain structures of a few hundreds of micrometers in size were reported [6]. On the scale of a few micrometers, single DWs have been resolved in the static limit by means of electron holography [7] with high spatial resolution. Additionally, we have shown that Kerr microscopy provides full-time and spatially resolved information about the dynamics of in-plane magnetic domains during the magnetization reversal on the scale of a few hundreds of micrometers [8]. Other authors have demonstrated that scanning Kerr microscopy can provide a spacial resolution down to 500 nm that can be used to image the magnetization dynamics in smaller structures [9]. Due to the low Curie temperatures (T_c) well below room temperature of most ferromagnetic semiconductors, it is of technical interest to study these materials in the highest possible temperature range just below T_c. In this work, we present a careful characterization of the temperature-dependent biaxial and uniaxial magnetic anisotropies in compressively strained GaMnAs and their influence on the evolution of the magnetic domain structure, thereby identifying limits for DW logic devices in the high-temperature regime. A preferential DW alignment is found to be linked to the change in the magnetic easy axis direction given by the temperature dependence of the uniaxial and biaxial anisotropy contributions. An increase in the number of domain nucleation centers is observed beyond a critical temperature where a biaxial-to-uniaxial anisotropy transition takes place. The dependence of this behavior on the geometry of the device is also presented.

The material under study consists of GaMnAs epilayers of 170 nm thickness grown on GaAs(001) substrates by molecular beam epitaxy (MBE). The compressive strain induced by the mismatch between the GaMnAs lattice constant and that of the underlying GaAs determines all the magnetization easy axes to lie within the surface plane [10]. The nominal Mn concentration is $(2.3 \pm 0.1)\%$, and this has been estimated on the basis of flux ratios. A more detailed description of the sample growth and material characterization has been given elsewhere [8]. The GaMnAs devices used in the Kerr microscopy experiments are Hall bars of 200 μm width fabricated by standard photolithography and ion milling.

1. Magnetic characterization of unpatterned, virgin GaMnAs epilayers

For a full characterization of the magnetic anisotropy within the GaMnAs epilayer, we performed temperature-dependent superconducting quantum interference device (SQUID) as well as magneto-optical Kerr effect (MOKE) measurements with magnetic fields applied in various in-plane directions. SQUID measurements were performed after cooling the sample in a field of 1000 Oe along a chosen direction. Thereafter the field was reduced to 50 Oe and the magnetization was measured in the respective direction with increasing temperature. The results are shown in figure 1(a) for fields along three directions [1$\bar{1}$0], [110] and [100]. Also plotted is the magnetization versus temperature $M(T)$ (figure 1(a), inset) in a saturating field of $H = 1$ T. From the temperature-dependent magnetic response at non-saturating fields of $H = 50$ Oe for different directions, the temperature dependence of the anisotropy constants can be estimated assuming a Stoner–Wohlfahrt coherent rotation of the magnetization following the total energy density $E(\varphi) = \frac{K_c}{4}\cos^2(2\varphi) + K_u \cos^2\varphi - MH\cos(\varphi - \varphi_H)$, where K_c and K_u are the biaxial and uniaxial anisotropy constants, M is the magnetization, H is the magnetic field and φ and φ_H are the angles of M and H with the [1$\bar{1}$0] direction. For each temperature the measured SQUID signal M^{SQUID} is determined simply by the equation system

$$\partial E/\partial\varphi = 0,\ (\partial^2 E/\partial^2\varphi > 0), \tag{1}$$

$$M^{\mathrm{SQUID}} = M\cos(\varphi - \varphi_H). \tag{2}$$

Here, M^{SQUID} is the measured projection of the magnetization $M(T)$ on the axis of the SQUID pick-up coils, which are aligned parallel to the magnetic field. While $M(T)$ is known from the SQUID measurement at saturating fields, K_u and K_c are temperature-dependent parameters to be derived by fitting. Assuming a magnetization dependence of the anisotropy constants close to $K_u = \alpha M^2$ and $K_c = \beta M^4$ [11], we can use equations (1) and (2) to fit the SQUID data, as shown in the inset of figure 1(b). The fits shown for the three directions [1$\bar{1}$0], [110] and [100] are derived using one and the same fit parameters $\alpha = 30.0$ and $\beta = 0.32$ in addition to the magnetization exponents 1.8 and 4.1 for the expressions of K_u and K_c, respectively. In figure 1(b), the temperature dependence of K_u and K_c is plotted as obtained from the fitting procedure. A clear crossover is observed from biaxial to uniaxial magnetic anisotropy at approximately 26 K where $K_u = K_c$. As a consequence, along the [110] direction the second derivative of the energy, $\partial^2 E/\partial^2\varphi$, changes sign at $K_u = K_c$ and the number of local minima in $E(\varphi)$ is reduced from 4 to 2 due to the disappearance of the biaxial-induced energy barrier in the [110] direction (see figure 1(c)). As extensively shown in magneto-transport measurements by Pappert *et al* [5], this crossover becomes directly visible in polar coercivity plots of figure 2, which summarize the coercive fields derived from MOKE hysteresis loops taken in different directions with respect to the [1$\bar{1}$0] crystal axis. The shape of the angular dependence of the coercivities at $T = 3$ and 27 K clearly confirms the change from a fourfold K_c dominated symmetry to a twofold K_u dominated symmetry at low and high temperatures, respectively. At low temperatures, in agreement with the literature, the biaxial fourfold symmetry leads to two-step reversals via intermediate local minima in $E(\varphi)$. Specifically for our samples, transitions at $T = 3$ K have been shown to be mediated by two individual DWs with DW angles $\Delta\varphi$ of $\sim 120^\circ$ and $\sim 60^\circ$, respectively [8], triggered at the coercive fields H_{c1} and H_{c2}. The reversal via an intermediate state is illustrated in the two right plots of figure 2(a), where $E(\varphi)$ is shown for fields $H = H_{c1}$ applied 15° away from the [110] and [1$\bar{1}$0] directions, respectively. For H_{c1}, the measured values at $T = 3$ K in the respective direction were taken. From the diagram it

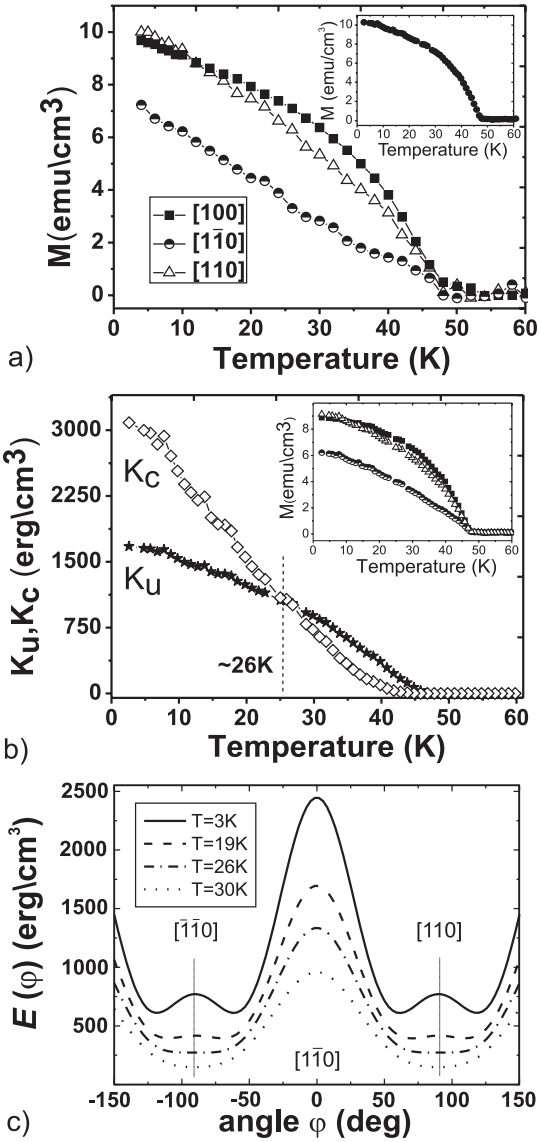

Figure 1. (a) Temperature-dependent SQUID measurements along the [1$\bar{1}$0], [110] and [100] directions in a field of 50 Oe. The inset shows the magnetization at a saturating field of 1 T. (b) Temperature dependence of K_u and K_c. The values have been derived by fitting the data shown in (a) using the saturated SQUID magnetization data and assuming Stoner–Wohlfahrt behavior and magnetization-dependent anisotropy constants $K_u = 30.0M^{1.8}$ and $K_c = 0.32M^{4.1}$. The fits for all directions are shown in the inset. (c) Energy density in the absence of a magnetic field for different temperatures. The plots are generated using the measured values for $K_u(T)$, $K_c(T)$ and the magnetization $M(T)$.

also becomes immediately evident that we expect H_{c1} measured close to the [110] directions to be higher compared to [1$\bar{1}$0] because in the former case the barrier that has to be overcome is governed by the larger uniaxial part K_u of the anisotropy landscape. Since we will later characterize DW transitions in detail using Kerr microscopy, we want to stress the fact that

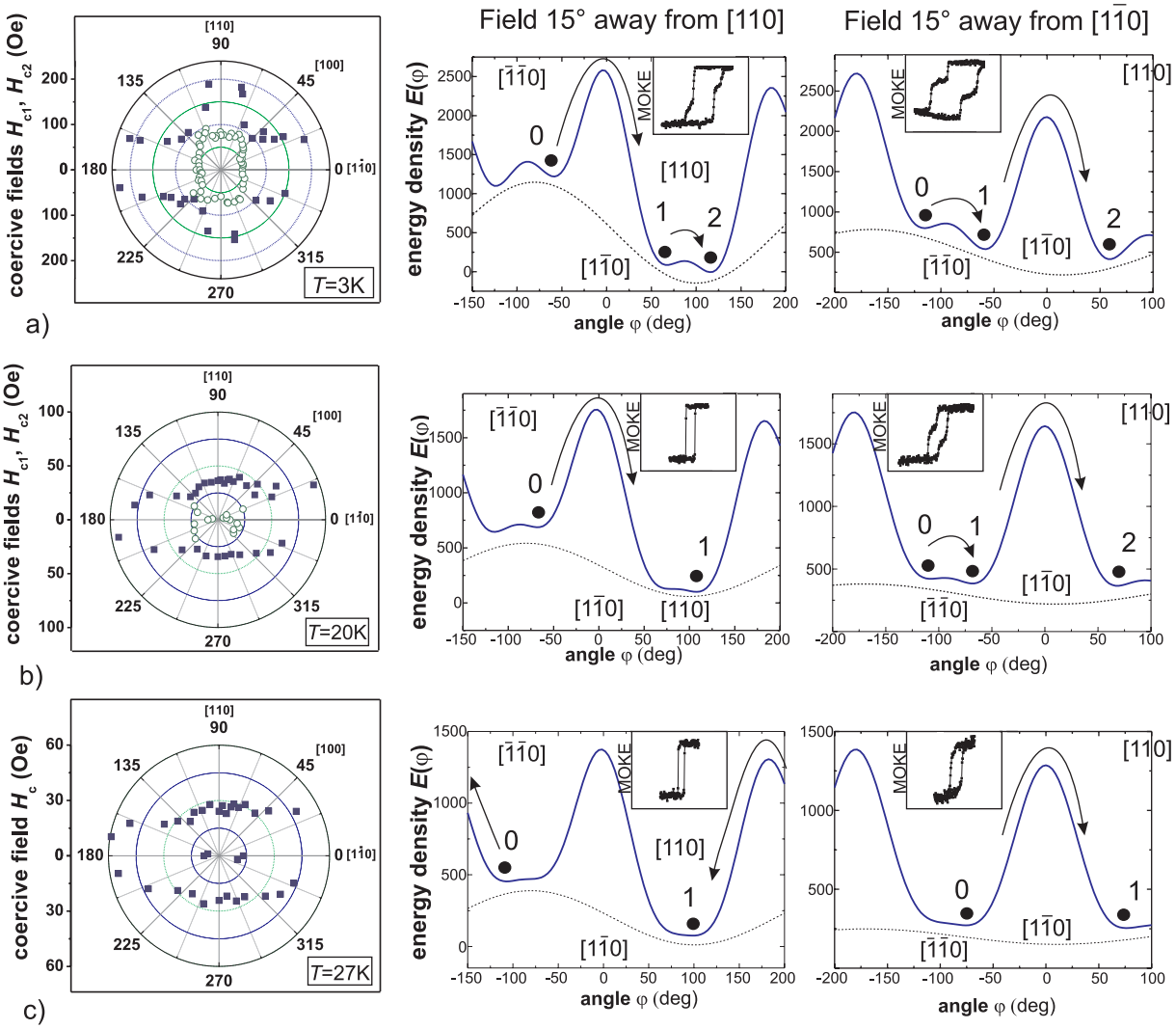

Figure 2. The polar plots on the left of (a), (b) and (c) show the measured coercivities as a function of the angle φ_H of the applied field with respect to the [1$\bar{1}$0] direction at the temperatures of 3, 20 and 27 K, respectively. At low temperatures, two coercive fields H_{c1} and H_{c2} appear, while at temperatures $T > 26$ K, the entire magnetic transition happens at one single field H_c. The two diagrams on the right of each of the three polar plots show the energy density $E(\varphi)$ at fields $H_{c1}(T)$ applied 15° away from the [110]($\varphi_H = 105°$) and [1$\bar{1}$0]($\varphi_H = 15°$) directions, respectively. The insets show the MOKE hysteresis measurement at the respective angles; all loops are plotted on the same scale (±300 Oe). As a reference, the Zeeman energy term is also plotted as dashed lines. The energy densities are plotted using the temperature-dependent values for K_u, K_c and the magnetization M.

measuring the coercivities at different φ_H can trigger magnetization transitions with either a clockwise (CW) or a counterclockwise (CCW) sense of rotation. From investigations into Fe/GaAs thin film systems with an equivalent magnetic anisotropy symmetry, it is known that

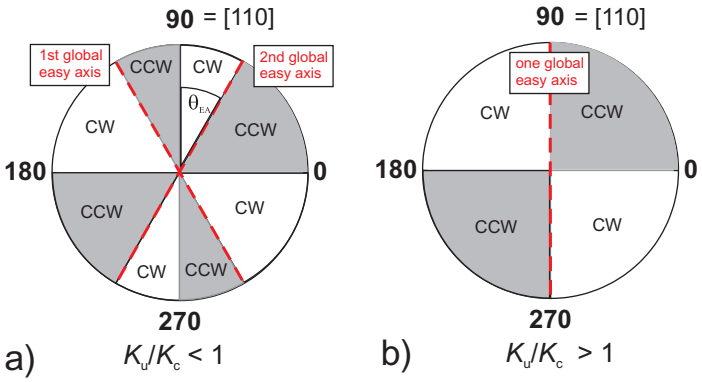

Figure 3. Magnetic field direction (φ_H) dependent change of the sense of the magnetization reversal process for (a) $K_u/K_c < 1$ and (b) $K_u/K_c > 1$. White areas represent CW rotation and gray areas represent CCW.

the sense of rotation changes whenever the magnetic field direction φ_H crosses a local minimum or a maximum in the magnetic energy landscape $E(\varphi)$ [20]. Therefore, as shown in figure 3(a), at low temperatures where $K_u/K_c < 1$, the sense of the transition changes eight times when φ_H is swept over the full angle range[4]. Four of the eight sign changes occur when the magnetic field direction crosses the two equivalent global easy axis directions located at angles $\pm\theta_{EA}(T)$ away from the [110] direction, as shown in figure 3(a). At high temperatures $T > 26$ K, in agreement with figure 2(c), only a single transition at H_c is observed and we expect DWs with angles of $\sim 180^\circ$. Accordingly, we expect that the sense of the transitions only changes sign four times during a full angle sweep of φ_H (see figure 3(b) for the case $K_u/K_c > 1$). At $T = 27$ K in a very narrow angle window close to the $[1\bar{1}0]$, low coercivities of about 15 Oe are found. When the field direction sufficiently deviates from the $[1\bar{1}0]$ axis, coercivities quickly jump to higher values larger than 30 Oe. In contrast, within an angle window $\pm 30^\circ$ away from the [110] direction, the coercivities are stable around ~ 30 Oe, indicating that in this region the magnetic reversal is highly reproducible and not sensitively dependent on the sample orientation. Consequently, applying the field along the [110] direction at different temperatures below and beyond the crossing point of K_u and K_c should allow for the observation of the transition between $\sim 120^\circ$ and $\sim 180^\circ$ DWs. From an application point of view, this direction is interesting since in this regime the transition was shown to be propagation dominated with a relatively small number of domains involved in the process [8].

2. Observation of temperature-dependent domain wall (DW) dynamics in patterned GaMnAs Hall bars

The Kerr-microscopic observation of magnetic domains was performed using the same procedure as described in [8]. The microscopy results focus on the temperature-dependent dynamics of DWs for magnetic fields applied close to the [110] direction. Before presenting these measurements, we would like to briefly discuss the expected change in the DW angle $\Delta\varphi$

[4] The change to the sense at the maxima of $E(\varphi)$ at $[1\bar{1}0]$ and [110] is directly visible when measuring the magneto-transport in our Hall bars. The transverse Hall voltage V_{xy} changes sign for measurements $\pm 5^\circ$ away from the respective directions.

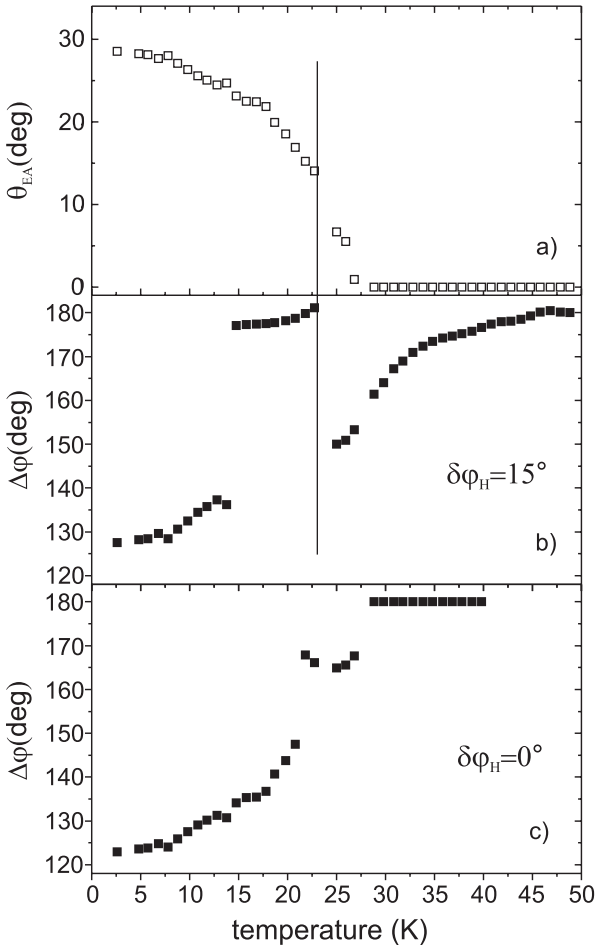

Figure 4. (a) Plot of the angle between the [110] axis and the closest global minimum direction versus temperature (open squares). The global easy axis reaches the [110] direction at about 26 K where $K_u = K_c$ (compare to figure 1). The corresponding DW angle for a transition via the uniaxial easy axis along [110] with $\delta\varphi_H = 15^\circ$ (b) and $\delta\varphi_H = 0^\circ$ (c) is also plotted (filled squares).

and sense of rotation with temperature as well as with increasing deviations $\delta\varphi_H$ from the [110] direction.

From simple symmetry arguments reflected in figure 3, it is evident that generally small deviations of $\pm\delta\varphi_H$ to both sides of the [110] direction will trigger DW transitions of opposite sense. However, despite the opposite sense in rotation, the absolute DW angles remain exactly the same. More specifically, at low temperatures $T < 26$ K and $\delta\varphi_H < \theta_{EA}$, CW (CCW) deviations lead to CW (CCW) transitions at H_{c1} and H_{c2}, whereas for $\delta\varphi_H > \theta_{EA}$, CW (CCW) deviations lead to a CCW (CW) transition. The angle θ_{EA} is shown in figure 3(a). For $T > 26$ K, CW (CCW) deviations always lead to a CCW (CW) transition. For a full understanding of DW dynamics at different temperatures, it is therefore important to trace the temperature-dependent global easy axis direction. To give an example of the influence of $\delta\varphi_H$ on $\Delta\varphi$, figure 4 shows the temperature-dependent angle $\theta_{EA}(T)$ of the global easy axis direction with respect to [110] at zero magnetic field together with the expected DW angle of the first transition at H_{c1} for

$\delta\varphi_H = 0^\circ$ and for a field deviation $\delta\varphi_H = 15^\circ$ with respect to [110]. The easy axis directions were obtained by tracing one of the two energy minima in $E(\varphi)$ closest to the [110] uniaxial easy axis (see figure 1(c)). $\theta_{EA}(T)$ is determined by $K_u(T)$ and $K_c(T)$ (see figure 1). As expected at $\sim$26 K, the temperature of the crossing between K_u and K_c, the global easy axis starts to be fully aligned with the [110] direction. The calculation of the DW angle of the first transition includes the temperature dependence of the coercive field applied close to the [110] direction. Coherent rotation effects in two domains separated by the DW are thus taken into account. The absolute DW angle $\Delta\varphi(T)$ for $\delta\varphi_H = 0^\circ$ and for the field deviation $\delta\varphi_H = 15^\circ$ shows two distinct jumps caused by the sequential destabilization of the initial and the final magnetization state of the transition. In the three middle row plots of figure 2, this effect is illustrated for the case $\delta\varphi_H = 15^\circ$. At about 20 K, the intermediate state of the CCW two-step transition becomes unstable and the magnetization rotates to the final state in a single step (in the MOKE hysteresis shown in the inset the intermediate step has vanished). $\Delta\varphi$ thus increases abruptly at this point. However, the CCW sense of the transitions is preserved. Finally, at temperatures $T \sim$23 K where $\theta_{EA} = \delta\varphi_H = 15^\circ$ (see figure 4), the sense of the transition changes to CW and the initial magnetization state rotates towards the $[\bar{1}\bar{1}0]$ direction, leading to a reduction in $\Delta\varphi$. As the temperature is further increased, the initial and final magnetization states approach the global easy axis direction along [110].

In the following, we prove on the basis of extensive Kerr microscopy measurements that the DW dynamics clearly reflect the change in magnetic anisotropy from a biaxial to a uniaxial dominated symmetry as a function of temperature.

2.1. DW alignment—charging of walls

The Kerr images in figures 5(a) and (b) (Hall-bar $\parallel$ [110]) and in figures 6(a) and (b) (Hall-bar $\parallel$ $[1\bar{1}0]$) show typical domain structures for the field applied along the [110] direction at 3 K and 27 K, respectively. For all four cases, two consecutive frames at times $t = t_0$ and $t = t_0 + \Delta t$ were extracted from a movie to picture the time evolution. Figures 5 and 6 demonstrate that the alignment of the DWs with respect to the [110] direction is clearly temperature dependent. While at low temperatures the DWs avoid the alignment with the [110] direction, they prefer the parallel alignment at higher temperatures in both cases. Only the DW nucleation behavior seems to be dependent on the Hall-bar orientation. Here, we observe that, only in figure 6 nucleation happens preferentially at the long sides of the Hall bar. We will discuss nucleation effects in detail in the next section.

In most magnetic systems the alignment of DWs is correlated to the surface divergence of the magnetization at the domain boundary due to magnetization components normal to the DW [12]–[14]. In general, this creates so-called magnetic charges proportional to $(\mathbf{M}_1 - \mathbf{M}_2) \cdot \hat{\mathbf{n}}$ at the DW boundary accompanied by a cost of stray field energy. Here, $\mathbf{M}_1$ and $\mathbf{M}_2$ are the magnetization vectors of the two domains separated by the DW and $\hat{\mathbf{n}}$ the wall normal facing towards domain 2. Hence, in our GaMnAs samples, in order to avoid magnetic charges, DWs should be aligned along [110] for the low temperature $\sim$120° DW transition with fields along [110]. At higher temperatures in the case of 180° DW transitions where the magnetization vectors $\mathbf{M}_1$ and $\mathbf{M}_2$ are collinear with the global easy axis along [110], we expect the system to try to avoid head-to-head type boundaries $\hat{\mathbf{n}} \parallel$ [110] with maximum amounts of magnetic charges [16]. Consequently, the observed DWs at 27 K show typical zigzag patterns throughout the reversal dynamics with $\hat{\mathbf{n}}$ pointing preferentially parallel to the $[1\bar{1}0]$ direction where

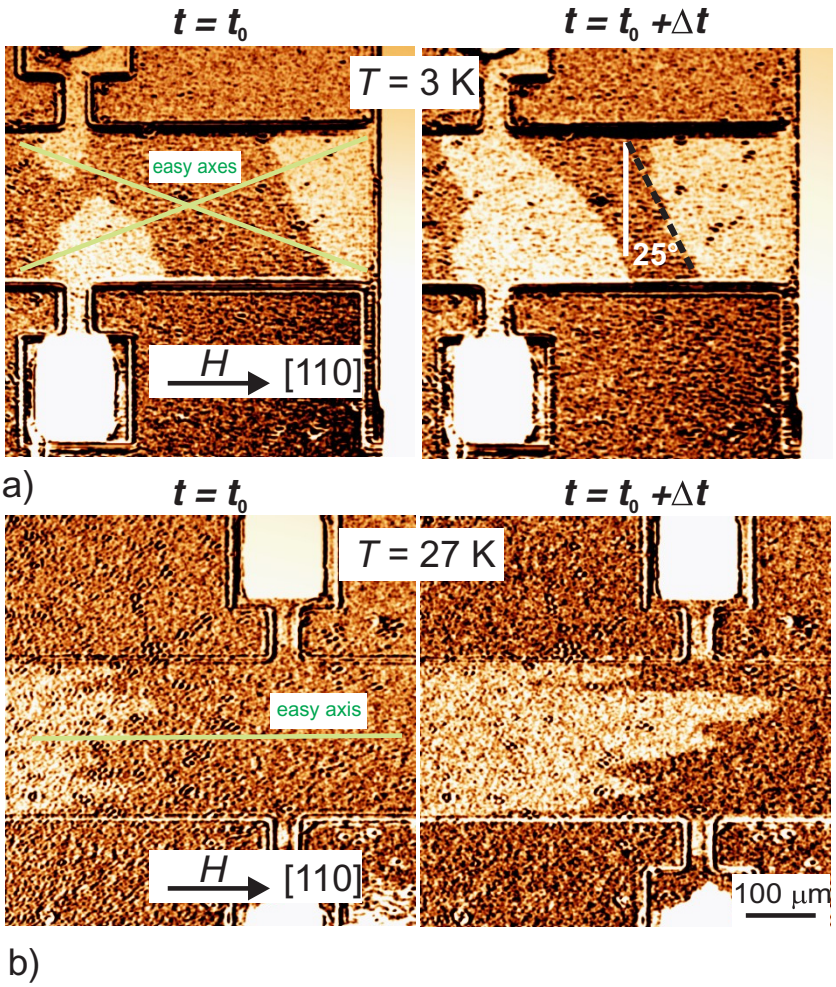

Figure 5. Kerr images of the domain structure at 3 K (a) and 27 K (b) (upper and lower images, respectively) in a Hall bar oriented along [110]. Left and right images are consecutive frames taken at times $t = t_0$ and $t = t_0 + \Delta t$ to picture the time evolution. The magnetic field is applied along [110]. The DW orientation changes significantly with temperature, while the number of nucleation centers is not strongly affected. The easy axis directions are indicated by green lines.

$(\mathbf{M}_1 - \mathbf{M}_2) \cdot \hat{\mathbf{n}} = 0$ holds. At low temperatures, however, out results are clearly not according to the above described model. As discussed, the reversal dynamics shown in figure 5(a) with the field applied along the [110] direction corresponds to a $\Delta\varphi \sim 120^\circ$ DW [8], where the initial and final magnetization states $\mathbf{M}_1$ and $\mathbf{M}_2$ are close to the two global easy axes at angles $\pm\theta_{EA} \sim \pm 30^\circ$ from the [110] direction (see figure 4). The preferential orientation of the DWs around 25° away from $[1\bar{1}0]$ observed in the Kerr images thus points to significant amounts of magnetic charges $\sim M \cos(25^\circ)$ accumulated at the DW. Figures 7(a) and (b) summarize the experimentally observed DW orientations for the case of 120° and 180° DW transitions at low and high temperatures together with the respective easy axis directions. We note at this point that the DW orientations are found to be the same in our virgin film samples and that therefore they are not a consequence of the Hall-bar patterning process.

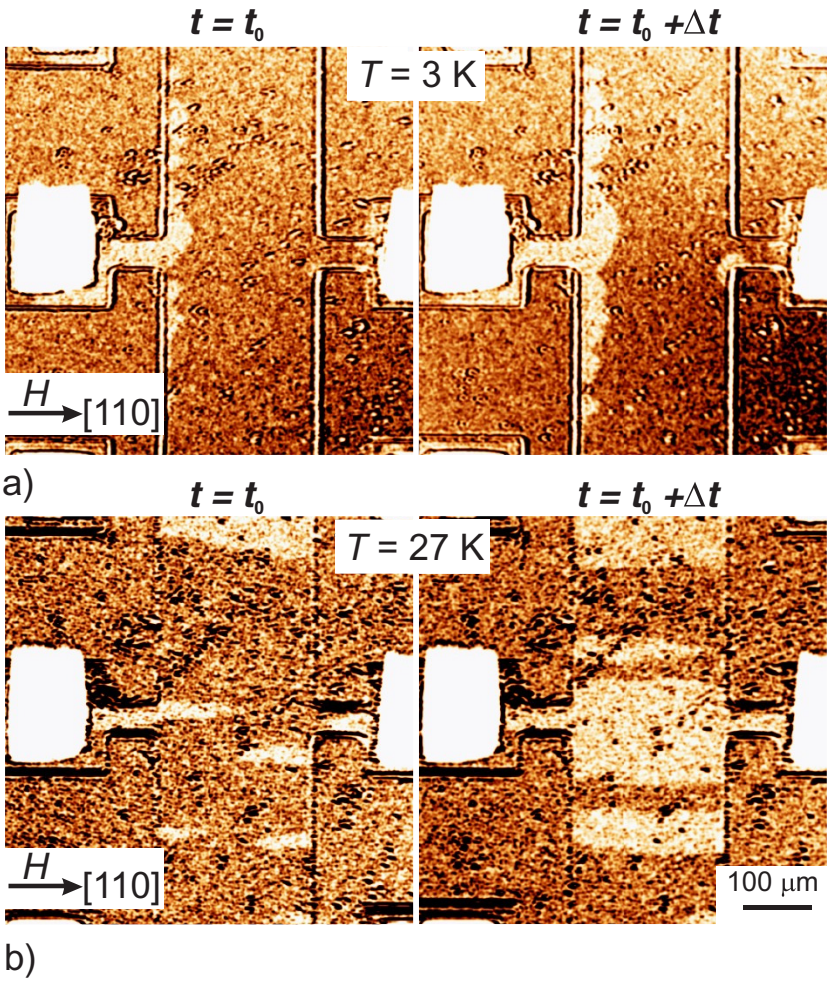

Figure 6. Kerr images of the domain structure under the same measuring conditions as for those shown in figure 5 but with the Hall bar oriented along $[1\bar{1}0]$.

Before we start to discuss the physics leading to the observed DW alignment behavior, it is helpful to estimate the expected contributions of the stray field to the energy density. In the diluted ferromagnetic semiconductor GaMnAs, the magnetization is about two orders of magnitude lower compared to typical $3d$ metal ferromagnets such as Fe and therefore stray field energy contributions to the total energy density are generally reduced by a factor of 10^{-4}. One of the consequences is that in GaMnAs films Néel walls are energetically preferred over Bloch walls up to relatively large film thicknesses d_{crit}. By this the system avoids magnetic charges at the film surfaces and encounters volume charges within the Néel wall. It has been shown that the critical thickness can be approximated by $d_{\mathrm{crit}} = 13.8\sqrt{A/4\pi M^2}$, where A is the exchange coupling constant [19]. With a typical value of $A = 4 \times 10^{-8}\,\mathrm{erg\,cm^{-1}}$ for GaMnAs and magnetization values of the order of $10\,\mathrm{emu\,cm^{-3}}$, one obtains a critical thickness of about $1\,\mu\mathrm{m}$ (compare to Permalloy where $d_{\mathrm{crit}} = 50\,\mathrm{nm}$). Thus, we can safely assume that the magnetic dynamics in our GaMnAs films of 170 nm thickness are governed by Néel-type walls in agreement with experiments by Sugawara *et al* [7].

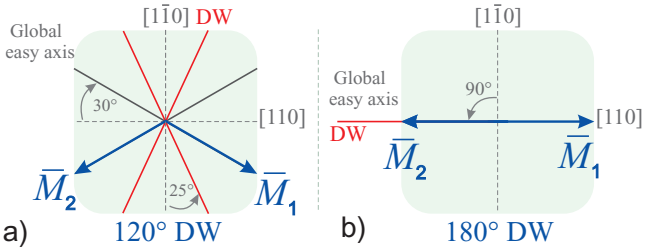

Figure 7. Diagram of the magnetization reversal process and observed DW orientation (red lines) at 3 K (a) and 27 K (b). The global easy axes are indicated by full gray lines and the [110] and [1$\bar{1}$0] crystal directions by dashed lines. The orientation of 180° DWs at higher temperatures is along the easy axis [110] (90° away from [1$\bar{1}$0]), whereas 120° DWs orient preferentially around 25° away from [1$\bar{1}$0].

The low magnetization value also reduces the stray field energy density ϵ_S caused by magnetic charges situated at a DW. It is given by $\epsilon_S = 2\pi((\mathbf{M}_1 - \mathbf{M}_2)\cdot\hat{\mathbf{n}})^2$ for an infinitely extended DW. For epitaxial Fe films of 150 Å thickness grown on GaAs substrates with a predominant cubic anisotropy $K_c > 0$ and large values ϵ_S of the order of $1 \times 10^6\,\mathrm{erg\,cm^{-3}}$, a strict preferential DW alignment according to the stray field minimization condition $\epsilon_S = 0$ has been reported by Gu *et al* [17]. The authors observe the alignment of 90° and 180° DWs with the hard and the easy axis, respectively, when the field is applied along the easy axis parallel to the cubic crystal symmetry direction. For our GaMnAs samples with low concentrations of Mn, however, stray field energy densities ϵ_S are only of the order of $100\,\mathrm{erg\,cm^{-3}}$ at most. Moreover, in thin films ϵ_S is further reduced due to the limited lateral extension of the DW when oriented perpendicular to the film. It can be shown that stray fields generated by magnetic charges in laterally confined Néel walls decay like $1/x^2$ at large distances away from the wall [18]. As a consequence for very thin films more complex Néel wall shapes occur. Here, total wall energies have to be evaluated numerically including exchange stiffness and magnetic anisotropy, which leads to solutions including isolated charged walls with $\epsilon_S \neq 0$ [19]. From calculations by Hubert [19] with therein defined dimensionless parameters $Q = K/2\pi M^2$ and $\lambda = 2Q\sqrt{A/K}/d$, one expects charged 120° DWs in our GaMnAs samples of thickness $d = 170\,\mathrm{nm}$ with $Q \approx 1$ and $\lambda \approx 1$ in accord with the results of our Kerr measurements at $T = 3\,\mathrm{K}$. DW charging effects similar to ours are visible also in epitaxial Fe films in the ultrathin film limit grown on GaAs. Although the authors of [17] did not discuss this aspect in detail, the film thickness-dependent cross-over from uncharged to partly charged 90° DWs clearly shows up in their Lorentz microscopy data for $d = 150$ Å and $d = 35$ Å, respectively [20]. In GaMnAs epilayers, Sugawara *et al* found both 90° Néel walls oriented along the [1$\bar{1}$0] direction and 20° away from the [1$\bar{1}$0] (see DW (iii) in figure 1(b) of [7]). The latter configuration again should correspond to a charged wall, although the authors did not comment on this issue. It should be noted, however, that since the Lorentz microscopy technique only permits the observation of domains close to the film edges where a non-magnetic reference signal is available, the local orientation of the DWs can also be affected by inhomogeneous morphology induced by the lithography process as well as flux closure processes.

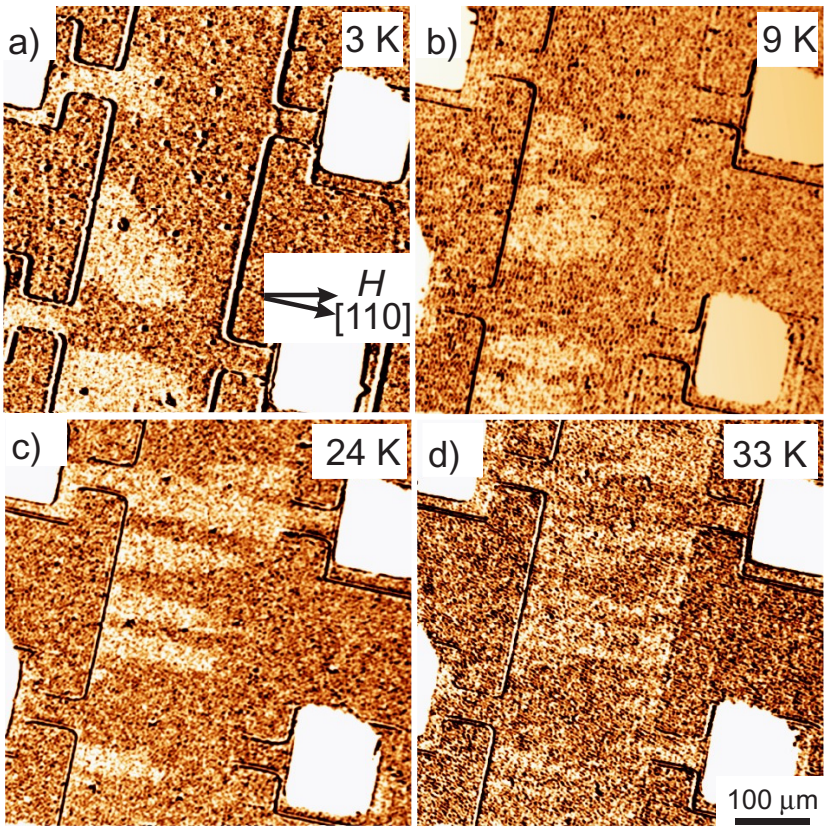

Figure 8. Kerr images of the domain structure for the field applied ∼15° away from [110] at 3 K (a), 9 K (b), 24 K (c) and 33 K (d).

2.2. *Temperature dependence of domain nucleation*

As mentioned in the previous sections, a clear asymmetry in the nucleation behavior is observed for Hall bars oriented in the [110] and [1$\bar{1}$0] directions (see figures 5 and 6). While in the former case, for both 120° ($T = 3$ K) and 180° ($T = 27$ K) DWs, a small number of domains occur and the contact pads of the Hall bar devices tend to serve as nucleation centers, for [1$\bar{1}$0]-oriented Hall bars, nucleation events happen preferentially at the long sides of the bar and appear to be larger in number.

In order to study the influences of geometry and temperature on the nucleation in more detail, we performed Kerr microscopy in small temperature steps on a Hall bar with its longitudinal axis along the [1$\bar{1}$0] axis. Below temperatures of ∼24 K, we observe that the number of domains involved in the transition remains fairly small and constant, as shown in figures 8(a) and (b) corresponding to temperatures of 3 and 9 K, respectively. However, beyond this temperature the number of nucleation events at the long sides of the Hall-bar edge grow dramatically and at the same time domains become increasingly elongated, as illustrated in the Kerr images in figures 8(c) and (d) taken at 24 and 33 K, respectively. The number of domains involved in the reversal process versus the temperature is plotted in figure 10 (open symbols) in a temperature range going from 3 to 33 K and show an exponential behavior. Due to the decreasing contrast in the Kerr signal with decreasing magnetization values, Kerr images could not be evaluated in the temperature range between 33 K and T_c.

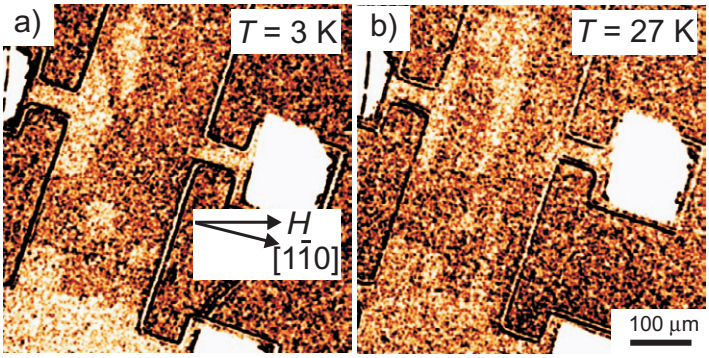

Figure 9. Kerr images of the domain structure for the field applied ∼20° away from [1$\bar{1}$0] at 3 K (a) and 27 K (b).

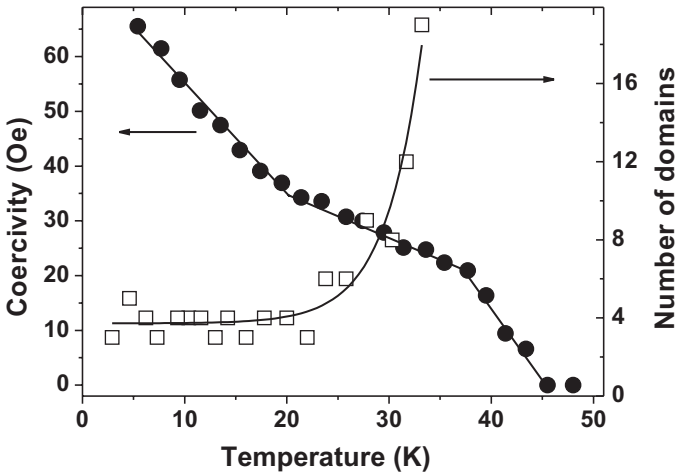

Figure 10. Temperature dependence of the coercive fields H_c along the [110] direction and number of domains involved in the magnetic reversal process, respectively.

Comparing the nucleation dynamics for the Hall bar oriented in the [110] and [1$\bar{1}$0] directions, it is evident that only ∼180° DWs appearing at temperatures around 25 K are strongly affected by the orientation of the Hall bar with respect to the crystal axis and field vector. Generally, the Kerr images in figure 8 confirm that for fields applied close to the [110] direction, nucleation of domains is happening at film edges facing the [110] direction. Indeed, as shown in figure 5(a) and (b), domains are never nucleated at the edges facing exactly the [1$\bar{1}$0] direction. Instead, nucleation in figure 5 happens at the square-shaped Hall-bar pads with two edges facing [110] or at the far Hall-bar ends (not visible in the Kerr images) again facing [110]. To prove that the asymmetry is indeed connected with the crystal orientation, we investigated a Hall bar patterned in the [110] direction with an applied field close to the [1$\bar{1}$0] direction (see figure 9). In agreement with our earlier work [8], we find multiple nucleation events within the film at low temperatures characteristic of ∼60° DW transitions and no preferential nucleation at the sides of the Hall bar. At high temperatures $T > 27$ K, again the domains are elongated along

the easy axis direction [110]. However, this time, preferential nucleation at the long sides of the Hall bar is not observed.

Anisotropic nucleation of domains in thin ferromagnetic films as observed in figure 8, where the observed preferred nucleation occurs at the Hall-bar sides $\parallel [1\bar{1}0]$, can have different origins.

Lithography-induced anisotropies. During the Hall-bar lithography process, differences in the edge profiles along [110] and $[1\bar{1}0]$ can be introduced. As an example, it is known that the wet etching process of GaAs exhibits different dynamics in the respective directions, leading to different edge profiles. However, the ion milling technique used in our case is a direction-independent process that generates a homogeneous edge profile in all the directions of the Hall bar. This was verified using x-sectional scanning electron microscopy. Also, lattice relaxation effects as observed at stripe edges [21, 22] that lead to local changes in the magnetic anisotropy energy $E(\varphi)$ should be equal in strength for edges $\parallel$ [110] and $\parallel [1\bar{1}0]$. We therefore claim that the observed asymmetric nucleation behavior cannot be a consequence of the Hall-bar patterning process.

Anisotropies through closure domains. Anisotropies in the nucleation rates can be induced by local dipolar fields, which decay like $1/x$ away from the edges and trigger flux closure domains. In micropatterned biaxial epitaxial Fe films on GaAs, DW transitions of 90° type are triggered preferentially at film edges where the rotation of the magnetization due to local dipolar fields has the same sense as the DW transition itself [23]. The local rotation of M can then be understood as a partial transition due to dipolar fields, which facilitates the domain nucleation induced by the external field H. Indeed, for the CCW 120° DW transitions shown in figure 8 (the H-field that induces the transition is slightly rotated CW from the global easy axis direction), we see nucleation at the edges $\parallel [1\bar{1}0]$ where the dipolar fields will rotate the magnetization vector M in the common sense. The opposite is true for edges $\parallel$ [110]. In the measurement configurations shown in figures 5(a) and 6(a), due to small deviations $\pm\delta\varphi_H$ of the field direction from [110], the sense of the transition can be either CW or CCW. However, independent of that, again the local rotation of M at the [110] edges is opposite in sense and therefore does not support nucleation in accord with our experimental findings. At higher temperatures $T = 24$ and 33 K (figures 8(c) and (d)), transitions proceed CW (the H-field that induces the transition is rotated CCW by 15° from [110]). Since the easy axis is exactly along [110], it is obvious that nucleation is again only facilitated at edges $\parallel [1\bar{1}0]$, where M produces maximum stray fields. However, we believe, in this case, that the sense of local rotation is not *a priori* predictable. At low temperatures and fields applied close to the $[1\bar{1}0]$ direction (CCW 60° DWs), we observe rather statistical nucleation within the entire device, as shown in figure 9. We tend to attribute this difference in nucleation dynamics to the reduced DW nucleation/propagation energy $\epsilon_{60°}$ with respect to 120° DWs [8]. Moreover, stray fields proportional to the projection $M\sin(\theta_{\mathrm{EA}})$ of $M(H = 0)$ on $[1\bar{1}0]$ are significantly reduced when compared to those propotional to $M\cos(\theta_{\mathrm{EA}})$ in figure 8.

The drastic increase in the number of domains $N(T)$ involved in the transitions above the temperature $T = 23$ K remains to be discussed. The problem resembles that of Fatuzzo's domain-nucleation model developed for ferroelectrics [24]. As described at the beginning of this section, the increase in N is accompanied by a change in the average width w of the domains, where w is the dimension of domains measured along $[1\bar{1}0]$ in figure 8. From the time-resolved

dynamics visible in our Kerr movies above $T = 24\,\mathrm{K}$, it is evident that after nucleation of a domain at the Hall-bar edges, DW propagation is mainly taking place in the [110] direction with little change in w of the respective domain. Following Fatuzzo, we therefore attribute the drastic increase in N to a complex interplay of temperature-dependent nucleation rates $\Gamma(T)$ at the film edges, a reduced DW mobility $\mu_{[1\bar{1}0]}$ along $[1\bar{1}0]$ and effects of coalescence of domains. If w_c is the average domain width at the coercive field H_c where 50% of the area of the film has switched, then the respective number of domains in a given section of the Hall bar with a length $l \parallel [1\bar{1}0]$ is approximately $N_c = l/2w_c$. Here, w_c will be a function of the mobilities along $\mu_{[110]}$ and $\mu_{[1\bar{1}0]}$ and the nucleation rates Γ. With this we can qualitatively understand the temperature-dependent nucleation dynamics. The Kerr data prove that with increasing temperature and especially for $T > 20\,\mathrm{K}$, the ratio between $\mu_{[110]}$ and $\mu_{[1\bar{1}0]}$ is significantly shifted toward propagation along [110], which assuming a constant Γ would reduce w_c and increase N_c. On the other hand, we expect Γ to increase with temperature according to a thermally activated process, which supports coalescence of domains at an early stage after nucleation. Generally, both a decrease in the mobilities and Γ leads to an increase in the coercive field H_c at constant sweep rates of the magnetic field. Indeed, the temperature dependence of H_c shown in figure 10 (full symbols) indicates a distinct decrease in slope at $T \approx 20\,\mathrm{K}$, which points toward a change in the mobilities and/or Γ (M decreases rather monotonously in this temperature range as shown in the inset of figure 1(a)). Sudden changes in $\mu_{[1\bar{1}0]}$ or Γ would not be unexpected since they occur in close proximity to the crossing point between K_u and K_c ($\sim 26\,K$), where the magnetic transitions change their character. Above the crossing temperature, we interpret the drastic increase in $N(T)$ to be mainly due to a monotonous reduction in $\mu_{[1\bar{1}0]}$. As previously mentioned, the dramatic change in the nucleation behavior roughly coincides with the onset of the uniaxial anisotropy dominated temperature regime and therefore may be linked to the structural seed of the uniaxial contribution to the magneto-crystalline anisotropy energy. The origin of the uniaxial anisotropy is still under debate. However, some authors tend to attribute it to an anisotropic dynamics during sample growth. This approach proposes that the Mn atoms are preferentially incorporated due to the layer-by-layer reconstruction of the surface during growth making the [110] and $[1\bar{1}0]$ directions inequivalent [6, 25]. It is well known that DW dynamics are highly sensitive to the presence of defects in the structure of the magnetic material where these defects can act both as domain nucleation centers and as DW pinning centers. Therefore, a preferential arrangement of the Mn atoms inside the structure potentially contributing to the appearance of the magnetic uniaxial anisotropy can also play an important role in the DW dynamics. This preferential incorporation of Mn could create an anisotropic arrangement of DW pinning centers for the [110] direction, with respect to the $[1\bar{1}0]$ direction, giving rise to the different DW velocities we observe along these two crystalline axes.

3. Conclusions

This work presents an extensive characterization of the temperature-dependent magnetic domain wall (DW) dynamics in Hall bars made from compressively strained GaMnAs and identifies limits for single DW logic devices in the high-temperature regime. The Kerr microscopy allows us to locally observe nucleation events of domains as well as the alignment and propagation behavior of DWs. A clear correlation of the preferential DW alignment with the temperature-dependent magnetic easy axis direction is found. The latter is determined by the temperature-dependent in-plane uniaxial and biaxial anisotropy energy contributions. At low temperatures,

magnetically charged DWs with DW angles considerably smaller than 180° are observed. Above the biaxial-to-uniaxial transition temperature, this charging effect is lost and DWs are oriented along the easy axis. Domain nucleation happens almost exclusively at Hall-bar edges aligned along the $[1\bar{1}0]$ uniaxial hard axis direction. This behavior is attributed to small demagnetizing field contributions at the edges of the device, which locally facilitate the magnetic transition and therefore nucleation of domains: the mechanism is asymmetric and favors nucleation at edges $\parallel [1\bar{1}0]$. Our extensive study of domain nucleation and propagation dynamics at variable temperatures in GaMnAs demonstrates that multi-domain states can be avoided by a suitable device geometry. This, together with our finding that the orientation of DWs can be tuned by the ratio between uniaxial and biaxial anisotropy energies, has important implications for potential applications in the field of magneto-logics and, in particular, for single DW devices where DWs are manipulated through spin-polarized currents.

Acknowledgments

We thank Professor H Kronmüller for valuable discussions and Ulrike Waizman for conducting the SEM measurements.

References

[1] Ohno H 1998 *Science* **281** 951
[2] Jungwirth T, Sinova J, Masek J, Kucera J and MacDonald A H 2006 *Rev. Mod. Phys.* **78** 809
[3] Dietl T, Ohno H, Matsukura F, Cibert J and Ferrand D 2000 *Science* **287** 1019
[4] Tang H X, Kawakami R K, Awschalom D D and Roukes M L 2003 *Phys. Rev. Lett.* **90** 107201
[5] Pappert K, Gould C, Sawicki M, Wenisch J, Brunner K, Schmidt G and Molenkamp L W 2007 *New J. Phys.* **9** 354
[6] Welp U, Vlasko-Vlasov V K, Liu X, Furdyna J K and Wojtowicz T 2003 *Phys. Rev. Lett.* **90** 167206
[7] Sugawara A, Kasai H, Tonomura A, Brown P D, Campion R P, Edmonds K W, Gallagher B L, Zemen J and Jungwirth T 2008 *Phys. Rev. Lett.* **100** 047202
[8] Herrera Diez L, Kremer R K, Enders A, Rössle M, Arac E, Honolka J, Kern K, Placidi E and Arciprete F 2008 *Phys. Rev.* B **78** 155310
[9] Hoffmann F, Woltersdorf G, Wegscheider W, Einwanger A, Weiss D and Back C H 2009 *Phys. Rev.* B **80** 054417
[10] Shen A, Ohno H, Matsukura F, Sugawara Y, Akiba N, Kuroiwa T, Oiwa A, Endo A, Katsumoto S and Iye Y 1997 *J. Cryst. Growth* **175/176** 1069
[11] Wang K Y, Sawicki M, Edmonds K W, Campion R P, Maat S, Foxon C T, Gallagher B L and Dietl T 2005 *Phys. Rev. Lett.* **95** 217204
[12] Hubert A and Schaefer R 1998 *Magnetic Domains: The Analysis of Magnetic Microstructures* (Berlin: Springer)
[13] Stewart K H 1954 *Ferromagnetic Domains* (Cambridge: Cambridge University Press)
[14] Tebble R S 1969 *Magnetic Domains* (London: Methuen)
[15] Horcas I, Fernández R, Gómez-Rodríguez J M and Colchero J 2007 *Rev. Sci. Instrum.* **78** 013705
[16] Vogel J, Cherifi S, Pizzini S, Romanens F, Camarero J, Petroff F, Heun S and Locatelli A 2007 *J. Phys.: Condens. Matter* **19** 476204
[17] Gu E, Bland J A C, Daboo C, Gester M, Brown L M, Ploessl R and Chapman J N 1995 *Phys. Rev.* B **51** 3596
[18] Kronmüller H 1965 *Phys. Status Solidi.* **11** K125
[19] Hubert A 1979 *IEEE Trans. Magn.* **15** 1251

[20] Daboo C, Hicken R J, Gu E, Gester M, Gray S J, Eley D E P, Ahmad E, Bland J A C, Ploessl R and Chapman J N 1995 *Phys. Rev.* B **51** 015964
[21] Wunderlich J *et al* 2007 *Phys. Rev.* B **76** 054424
[22] Wenisch J, Gould C, Ebel L, Storz J, Pappert K, Schmidt M J, Kumpf C, Schmidt G, Brunner K and Molenkamp L W 2007 *Phys. Rev. Lett.* **99** 077201
[23] Ebels U, Adeyeye A O, Gester M, Daboo C, Cowburn R P and Bland J A C 1997 *J. Appl. Phys.* **81** 4724
[24] Fatuzzo E 1962 *Phys. Rev.* **127** 1999
[25] Welp U, Vlasko-Vlasov V K, Liu X, Furdyna J K and Wojtowicz T 2004 *Appl. Phys. Lett* **85** 260